Title: Spatiotemporal input reorganization and enhancement of input-output gain sharpen cortical direction selectivity during development.

Abbreviated title: Cellular mechanisms of direction selectivity

Authors: Arani Roy[1,2], Jason J. Osik[1,2], Benyamin Meschede-Krasa, Wesley Alford, Stephen D. Van Hooser[1,2,3*]

1: Department of Biology
2: Volen Center for Complex Systems
3: Sloan-Swartz Center for Theoretical Neurobiology
Brandeis University, Waltham, MA 02454 USA

Corresponding author:
*Stephen D. Van Hooser, vanhooser@brandeis.edu
Brandeis University, 415 South St. MS008, Waltham, MA 02454 USA

Number of Pages: 36
Number of Figures and Tables: 5 Figures, 0 Tables

Conflicts of interest: The authors declare no competing financial interests.

Contributions: AR, JJO, and SDV designed experiments; AR, JJO, BMK, and WA collected data; AR, JJO and SDV performed data analysis; AR wrote the manuscript with input from SDV and JJO.

Keywords: primary visual cortex; direction selectivity; cortical development; sensory experience; spatiotemporal receptive fields; intrinsic excitability; spike threshold; gamma oscillation.

Abstract

In the primary visual cortex (V1) of carnivores and primates, early visual experience shapes the development of functional properties such as selectivity for direction of motion. However, it remains unclear which aspects of the cortical circuitry - synaptic and/or cell-intrinsic - are molded by the visual activity, and how. Therefore, we performed in vivo intracellular recordings from V1 simple cells in visually naive and experienced ferrets, and computed their membrane potential (Vm) spatiotemporal receptive fields and Vm-to-spike input-output transfer functions. Comparison across the two developmental stages revealed marked reorganization of inputs and a sharp enhancement of input-output gain in the experienced state, leading to prodigious amplification of direction selectivity at the spiking level. Simultaneously, we detected a lowering of spike thresholds and an intensification of gamma-band Vm oscillations, which might explain the enhancement of spiking. Thus, direction selectivity develops through combined processes of synaptic re-wiring and maturation of cell-intrinsic properties.

Introduction

The primary sensory cortices construct a representation of the physical world by integrating neural response selectivities for distinct sensory features. The receptive fields underlying these feature selectivities arise through a combination of the precise patterns of synaptic inputs received by cortical neurons and their intrinsic cellular properties. A cortical neuron receives thousands of cortical and sub-cortical synaptic inputs and generates a spiking output that reflects its response selectivity. The cell-intrinsic properties gate the input-output transformation by controlling how the neuron summates its inputs and then maps the summed input to a spiking output. Determining how the synaptic input patterns and the cell-intrinsic properties of cortical neurons evolve during development is a key component to understanding how a mature cortical circuit performs computations in general.

In the primary visual cortex (V1), neuronal responses are characterized by selectivity for two features of visual stimuli: orientation (orientation selectivity, OS) and direction of motion (direction selectivity, DS)[1-3]. In ferrets, a small carnivore, OS develops early through innately-specified processes that do not require visual experience, and consequently V1 neurons exhibit significant OS already at the time of eye-opening[4-6]. In contrast, DS – defined as a neuron's preference for one of the two directions of motion orthogonal to its preferred axis of orientation – typically develops over a period of 1-2 weeks after eye opening through a process that requires visual experience, and does not form in dark-reared or strobe-reared animals[4,5,7-9]. In direction-selective simple cells of V1 in visually experienced animals, the spatially selective synaptic inputs activate the cell with varying latencies in a specific temporal order[10-12]. These subthreshold inputs are summed linearly, thereby generating direction-selective responses at the subthreshold level, and are then passed through a threshold non-linearity to obtain a direction-

selective spiking response[13-15]. During development, an increase in DS at the level of spiking could be brought about by an improved spatiotemporal summation[16,17], an enhancement of input-output transfer non-linearity[13], or both. During the first weeks of vision, visually-driven neural activity must transform the patterns of synaptic connectivity and the cellular properties of simple cells to instantiate these changes and lead to enhanced DS. To understand this process, it is necessary to study the evolution of the input patterns and the input-output transformations of simple cells over the period when DS emerges.

Therefore, we carried out in vivo sharp intracellular recordings from V1 simple cells in visually naïve and experienced ferrets and compared the spatiotemporal patterns of synaptic inputs as well as the input-output transfer functions across these developmental stages. Comparison of the simple cell spatiotemporal receptive fields (STRFs) between naïve and experienced ferrets revealed that there were significant reorganizations in the spatiotemporal patterns of inputs in the experienced animals, leading to more optimal linear summation of inputs and consequently to a modest increase in Vm responses to the preferred direction of motion. Further, the slope of the non-linear Vm-to-spike transfer function underwent sharp enhancement during the same period of development. This enhancement in gain was brought about by lowering of spike threshold and increase in high frequency oscillations of Vm in the experienced animals. As a result of these modifications, the modest improvements in Vm responses induced by STRF rearrangements mapped on to a steeper input-output transfer curve in the experienced animals, leading to a sharp enhancement in DS at the spiking level.

Results

To study the subthreshold mechanisms of development of direction selectivity (DS) in the primary visual cortex (V1) of ferrets, we carried out *in vivo* intracellular recordings in V1 using sharp microelectrodes. Experimental animals were split in to two age groups: visually naïve ("naïve": age P30-34, n = 10 animals, 23 cells) and visually experienced ("experienced": age P40-60, n = 11 animals, 29 cells). Cells were recorded under isoflurane anesthesia while visual stimuli were displayed on a computer monitor. Sinusoidal gratings at varying orientation angles (in steps of 30 degrees) drifting in either of the two directions orthogonal to the axis of orientation were used to map orientation and direction tuning of neurons. The degree of orientation and direction selectivity were expressed using orientation selectivity index (OSI) and direction selectivity index (DSI), respectively, both of which varied between 0 to 1 (see Supplementary methods). Because V1 simple cells have a substantial linear response[15], Vm and spike responses of these neurons to drifting grating stimuli are periodically modulated following the temporal frequency of the grating[18]. Simple cells are typically distinguished from complex cells by comparing the fundamental (F1) and the DC components (F0) of the responses[14,18,19]. We first converted the Vm and spike responses of each recorded neuron to the frequency domain using Fast Fourier Transform (FFT) and then analyzed all response properties for the F0 and F1 components separately as well as combined (F0+F1). We calculated Vm and spike modulation ratios by dividing the amplitude of the F1 component by that of the F0 component of the respective responses. Cells with spike modulation ratio equal to or greater than 1 were classified as simple, while the rest were categorized as complex (see **Supplementary Figure S1**). Neurons that did not fire sufficient spikes were classified as simple if their Vm modulation ratio was greater than 0.5. According to this classification, our data set contained 26 simple cells (10 in

naïve and 16 in experienced groups) and 26 complex cells (13 each in naïve and experienced groups). In the following sections, we first describe the various analyses performed on the simple cells, while relevant data from the complex cells are provided in supplementary figures S3, S7-9.

Emergence of Direction Selectivity following visual experience

We saw a sharp rise in visually-evoked spiking responses from both simple and complex cells of the experienced animals. The increased responsivity could be detected in two ways. First, the fraction of cells that fired action potentials in response to drifting grating stimuli was significantly higher in the experienced group (simple: naïve, 7/10; experienced, 16/16; $p < 0.05$, complex: naïve, 7/13; experienced, 13/13; $p < 0.05$, Fisher Exact test). Thus, every recorded cell in the experienced group fired action potentials, but 9/23 cells in the naïve group did not fire any action potentials at all, even though subthreshold visual responses could be detected in these neurons. Second, the magnitude of spiking responses to the preferred direction of motion was significantly stronger in the experienced group (**Supplementary Figure S2**; naïve vs experienced, for both simple and complex cells, $p = 0.001$, Wilcoxon Rank Sum (WRS) test). Therefore, spiking responses dramatically increased in the visually experienced animals.

Direction selectivity, measured both at the sub- and suprathreshold levels, increased in the experienced animals. **Figure 1A** shows an example simple cell each from a naïve and an experienced ferret. The neuron from the naïve ferret (**Figure 1A**, left panel) responded strongly to horizontal gratings, irrespective of whether they were moving upward or downward, while showing only weak subthreshold responses to vertical gratings. In contrast, the neuron from the experienced ferret (**Figure 1A**, right panel) strongly responded only to vertical gratings drifting to the right while responding minimally to all other stimuli. Thus, while both neurons exhibited

orientation selectivity, only the experienced neuron exhibited direction selectivity as well. To describe the feature selectivity of these neurons, we plotted their F0 and F1 response magnitudes for each direction of motion in the form of tuning curves. In the tuning curves of the naïve neuron (**Figure 1B**, left panel), two strong peaks in the direction space separated by ~180 degrees signified existence of orientation selectivity along with low direction selectivity. In contrast, for the experienced neuron (**Figure 1B**, right panel), one strong peak in the direction space signified both high orientation and direction selectivity.

To quantify the degree of direction selectivity, we calculated a direction selectivity index (DSI) from the sub- and suprathreshold responses for each cell (see Supplementary methods). In simple cells (for analysis of complex cells, see **Supplementary Figure S3**), the total DSI (F0+F1) increased significantly from the naïve to the experienced group for both sub- and suprathreshold responses (**Figure 1C**, top, Vm: naïve: mean = 0.15 +/- 0.04, n = 10; experienced: mean = 0.36 +/- 0.05, n = 16; $p < 0.01$, WRS test; bottom, spike: naïve: mean = 0.34 +/- 0.07, n = 7; experienced: mean = 0.73 +/- 0.05, n = 16; $p = 0.001$, WRS test). These data are consistent with previous studies showing that in V1 DS is low around the time of eye-opening and gradually increases over the following 1-2 weeks[5,8,9].

In a majority of simple cells, the DSI for spiking responses were higher than the DSI for Vm responses. A pairwise comparison of Vm and spike DSI within each neuron revealed that the spike DSI was significantly higher than Vm DSI in both the naïve and the experienced groups (**Figure 1D**; naïve, $p = 0.04$, n = 7; experienced, $p < 0.001$, n = 16; signed rank test). Therefore, in both groups of animals, the outputs of V1 simple cells were more sharply tuned for direction than their summed inputs, hinting at non-linear transformation from Vm inputs to spiking outputs[13,18].

It is evident from the individual responses and the tuning curves in **Figure 1A** and **1B** that, in addition to the linear response component (fundamental or F1) that modulates following the stimulus contrast, the responses of simple cells also contain a significant non-linear component (DC or F0: the elevation of Vm from the baseline floor). To test if the developmental enhancement of DSI in the simple cells were restricted to one of these two components or affected both, we calculated DSI separately for the F0 and F1 response components. F0 and F1 DSI for both sub- and suprathreshold responses in the experienced group were significantly higher than the naïve group, demonstrating that selectivity of both the linear and the non-linear components of simple cell responses underwent enhancement following visual experience (**Figure 1E**; F0: Vm: naïve: mean = 0.13 +/- 0.03, n = 10; experienced: mean = 0.27 +/- 0.04, n = 16; p = 0.02, WRS test; spike: naïve: mean = 0.36 +/- 0.08, n = 7; experienced: mean = 0.7 +/- 0.05, n = 16; p = 0.004, WRS test; F1: Vm: naïve: mean = 0.28 +/- 0.05, n = 10; experienced: mean = 0.53 +/- 0.07, n = 16; p = 0.03, WRS test; spike: naïve: mean = 0.33 +/- 0.07, n = 7; experienced: mean = 0.76 +/- 0.05, n = 16; p = 0.001, WRS test).

An increase in DSI could be realized either by an increase in responses to the preferred direction, a decrease in responses to the null direction, or both. In order to delineate the response dynamics underlying the enhancement of DSI, we analyzed the Vm and spiking response amplitudes to the preferred and the null direction stimuli for each simple cell. The total (F0+F1) responses to the preferred and null stimuli were compared between the naïve and experienced groups, separately for Vm and spiking responses (**Figure 1F**). At the level of Vm (**Figure 1F**, top), the null responses (left) do not show any significant change over development, whereas the preferred responses (right) show a modest but significant increase from the naïve to the

experienced group (null, naïve: mean = 10.9 +/- 1.4, n = 10; experienced: mean = 10.6 +/- 1.05, n = 16, p = 0.8, WRS test; preferred, naïve: mean = 12.7 +/- 1.3, n = 10; experienced: mean = 17.1 +/- 1.2, n = 16, p = 0.02, WRS test). At the level of spiking (**Figure 1F**, bottom), a similar pattern was observed (null, naïve: mean = 4.9 +/- 1.9, n = 10; experienced: mean = 8.3 +/- 2, n = 16, p = 0.15, WRS test; preferred, naïve: mean = 7.01 +/- 2.4, n = 10; experienced: mean = 28.6 +/- 4.2, n = 16, p < 0.001, WRS test). Therefore, the increase in DSI following visual experience was driven by an increase in responses to the preferred direction of motion and not by a decrease in response to the null direction of motion. Notably, while this increase was modest (35%) at the Vm level, at the spiking level the enhancement of responses to the preferred direction was dramatic (302%).

In summary, visual experience during the 2-4 weeks following eye opening led to a modest increase in Vm responses to the preferred direction of motion, but, this modest increase in Vm responses led to a much stronger response enhancement at the spiking level, thus leading to a robust increase in spike DSI.

It is unclear whether this large enhancement of spike DSI is simply a reflection of the modest enhancement of Vm DSI alone, or whether other mechanisms were involved in amplifying the sub-threshold DSI enhancement. An improved spatio-temporal summation of sub-threshold inputs could account for the observed Vm DSI enhancement. While this alone might fully explain the spike DSI enhancement, other mechanisms such as developmental increase in input-output gain could also further amplify the modest Vm DSI enhancements and lead to greater spike DSI. To parse out these possibilities, we carried out two sets of analyses. First, to compare spatiotemporal summation of Vm between naïve and experienced groups, we used reverse correlation of Vm to sparse white noise to map out the Vm spatio-temporal receptive fields

(STRFs)[11,12,20-22] of the simple cells in our data set. Second, we constructed the input-output transfer functions of all V1 simple cells by comparing their average spike outputs to the average Vm levels[13,14], and tested if the input-output gain underwent developmental enhancements.

Mapping spatio-temporal receptive fields of simple cells

Intracellular recordings revealed that the Vm responses became more direction-selective in the visually experienced animals (**Figure 1BCEF**). In simple cells, direction selectivity is thought to arise from spatially selective inputs activating the cell at temporally varying latencies[10,15,16,23]. According to this model[24,25], a direction selective neuron is maximally activated when its inputs selective for specific spatial locations within the receptive field are activated by a moving stimulus in a specific temporal order – the inputs with the longest latencies activating first and inputs with progressively shorter latencies sequentially activating thereafter. This spatio-temporally sequenced order of activation ensures that the subthreshold inputs activated by the preferred direction of motion arrive at the soma simultaneously and achieve maximal summation, leading to a strong response. In contrast, a stimulus moving in the null direction activates the shortest latencies first followed by progressively longer latencies, thereby leading to suboptimal summation of activity, and consequently lower responses in the postsynaptic neuron. A direction-selective simple cell with its inputs organized in this manner exhibits a slant in its spatio-temporal receptive field (STRF). Could the lower Vm responses detected in visually naïve ferrets be a consequence of immature, non-slanted STRF structures? To test this idea, we computed the Vm STRFs in a subset of V1 simple cells from our data set (naïve: n = 8, experienced: n = 12), and compared various shape parameters describing the STRF structure.

Once a simple cell's preferred orientation was calculated from its tuning curve (**Figure 1B**), linear STRFs were computed by reverse correlating the neuron's spike-filtered Vm responses to

a sparse 1-dimensional white noise stimulus[13,21,22]. The noise stimulus consisted of black, white and gray bars, angled at the cell's preferred orientation, that changed pattern every 100 milliseconds (see Supplementary methods, **Supplementary Figure S4**). Therefore, for every spatial location on the monitor, the contrast trace varied between 1, 0 and 1 over time, and this trace was cross-correlated with the spike-filtered Vm trace recorded during the stimulus. High cross-correlation values were obtained if a white bar (contrast 1) led to increased Vm or a black bar (contrast -1) led to decreased Vm (ON subunit), and low cross-correlation values were obtained if a white bar led to decreased Vm or a black bar led to increased Vm (OFF subunit). For every spatial location the cross-correlation values were plotted at varying lag times, thereby allowing assessment of the latencies at which the high or low cross-correlation values were obtained. Because visually driven spiking activity was weak in naïve ferrets, we focused our analysis primarily on the Vm responses, for which a reliable STRF could be computed for every simple cell tested.

Figure 2A shows Vm STRFs of 2 cells recorded from a naïve ferret (cell # 102 and 121) and 2 cells recorded from a experienced ferret (cell # 60 and 80). Consistent with previous findings[11-13,16], the STRF subunits from the high-DSI neurons in experienced animals were slanted in space-time. For cell # 60, gratings moving from right to left on the monitor would activate the inputs with longer latencies first, progressively moving to shorter latencies as the grating moves across the visual field, thereby leading to maximal response. Stimulus moving from left to right, on the other hand, will activate the shorter latency inputs followed by the longer latency inputs, thereby leading to sub-optimal responses. The STRF of the Cell # 80 was also slanted, albeit in the opposite direction, thus signaling that this cell would prefer gratings moving from left to right on the monitor. Indeed, the preferred directions obtained from the tuning curves of these cells

matched the direction preference predicted by the STRFs. The STRFs from the low-DSI neurons in naïve animals were not completely unstructured and exhibited several experienced properties such as alternating ON and OFF subunits and a small slant in space-time. However, the STRF subunits from the experienced cells were longer and narrower in profile, and relatively more slanted in space-time.

To rigorously quantify the degree to which STRF subunit structure differed between naïve and experienced animals, we fitted ellipses to the individual ON and OFF subunits[26] and compared various shape parameters of these ellipses (see **Supplementary Methods**). We chose a set of nine parameters that adequately captured the relevant spatial and temporal characteristics of the STRFs (**Figure 2B**) – 'eccentricity': eccentricity of the fitted ellipse; 'major axis': the length of the major axis of the fitted ellipse; 'minor axis': the length of the minor axis of the fitted ellipse; 'orientation': the angle the ellipse subtended on the space (x-) axis; 'area': the full area covered by the ellipse, in pixels; 'spatial extent': projection of the ellipse on the space axis; 'temporal extent': projection of the ellipse on the time/latency axis; 'minimum latency': the lower bound of the fitted ellipse on time axis signifying the shortest latency response in the STRF; and 'maximum latency': the upper bound of the fitted ellipse on time axis signifying the longest latency response in the STRF. Wilcoxon rank sum test comparisons revealed that 6 out of these 9 parameters were significantly different between the naïve and the experienced groups: eccentricity, major axis, minor axis, orientation, temporal extent and minimum latency. The shape parameter that is most relevant to direction selectivity is the eccentricity of the ellipses describing the STRF subunits. If STRF subunits are broad along the minor axis of the ellipse, they will enable some response summation from stimuli moving in either direction, thus leading to weaker direction selectivity. Also, if STRF subunits are short along the major axis of the

ellipse, there might not exist sufficient latency differences to facilitate differential input summation. Therefore, to optimally support high direction selectivity, STRF subunits would have to be narrow on the minor axis and elongated on the major axis, which would result in high eccentricity. Consistent with this idea, we found that the eccentricity measured from the experienced subunits were significantly higher ($p = 0.001$), and was caused by both a longer major axis ($p = 0.03$) and a shorter minor axis ($p = 0.03$). Also, the subunits from the experienced animals subtended a smaller angle on the space axis (orientation: $p = 0.005$), which would predict the cells from experienced animals to be tuned to higher motion velocities, consistent with data from actual V1 recordings in cats[17]. The overall area ($p = 0.6$) and the spatial projection ($p = 0.35$) of the subunits did not significantly differ. However, the projection on the latency axis was significantly longer in the experienced group ($p = 0.04$), suggesting that a longer range of response latencies became available in the experienced animals. This extension of the latency range was achieved solely by stretching the STRF subunits towards the lower latency side: while the maximum latencies of the subunits were not significantly different ($p = 0.3$), the minimum latencies were significantly lower in the experienced group ($p = 0.05$). This suggests recruitment of lower latency inputs in the experienced animals[27]. Consistent with this view, we found that the Vm response latency distributions were significantly shifted towards lower latencies in the experienced animals (**Supplementary Figure S5**).

If the changes in Vm STRF structure resulted in improved discrimination between preferred and null directions of motion, the STRF structure parameters should correlate with Vm DSI measured in each cell. Therefore, we computed linear correlations between cell-averaged shape parameters and the cells' Vm DSI values (**Figure 2C**). We found that the Vm DSI of the cells increased with increasing 'narrowness' of the subunits (longer 'major axis', shorter 'minor axis'

and higher ‘eccentricity’) and decreasing minimum latencies accessible (lower ‘min latency’). Other parameters did not show significant correlation. These data further corroborate the idea that narrower spatio-temporal input profiles and availability of shorter-latency inputs exert a strong impact on directional summation of inputs in simple cells of experienced animals, thereby leading to higher direction selectivity.

We tested the linearity of spatiotemporal input summation in the simple cells in two ways. First, we converted the STRFs into frequency domain using Fast Fourier Transform and generated predicted Vm DSI from these frequency-domain STRFs[13] (see Supplementary methods). Across naïve and experienced animals, there was significant linear correlation between the predicted and actually measured Vm DSI (**Supplementary Figure S6A**), signifying that a third of the variance in Vm direction selectivity could be explained by the variance in linear spatiotemporal properties. Second, we convolved the STRFs for each neuron with the white noise stimulus presented during STRF mapping to predict the Vm trace for each trial. The linearly predicted Vm traces captured closely the modulation of the actually recorded Vm traces, though not entirely (**Supplementary Figure S6B**). The average R^2 per cell for linear correlation between predicted and actual Vm traces were indistinguishable between naïve and experienced groups and the overall R^2 was 0.37. Thus, according to both methods, about a third of the variance in Vm dynamics could be explained by the linear STRFs, leaving the rest of the variance to non-linear and stochastic processes. But this sizable non-linear component was not distinguishable between naïve and experienced groups, thereby ruling out altered non-linearity of sub-threshold summation as a potential mechanism by which Vm DSI is enhanced in the experienced group.

In summary, following visual experience, the Vm receptive fields exhibit marked reorganization involving narrowing of the space-time profile and recruitment of lower latency inputs, leading to improved discrimination of directional inputs at subthreshold level and thus a more direction-selective Vm response.

Mapping input-output transfer functions of simple cells

Sharp rise in visually-evoked spiking in the experienced animals (**Supplementary Figure S2, Figure 1F**) raised the possibility that excitability of the V1 simple cells is enhanced during development, contributing further to increased spike DSI. To test this idea, we calculated mean Vm and mean firing rates in 30 msec bins during the preferred orientation stimulus trials and plotted them against each other (Voltage-Firing or V-F plots; **Figure 3A**, see Supplementary methods). **Figure 3B** shows example V-F plots of 2 cells each from the naïve (left column) and the experienced (right column) groups. For each curve, average Vm levels relative to pre-stimulus baseline is plotted on the x axis and average firing rates expressed during those epochs of Vm responses is plotted on the y axis. The individual points were then fitted with a hyperbolic tangent function that captured the nonlinearity of the relationship both at the low and high Vm levels, and those fitted curves are plotted with the solid lines. Several observations can be made from these exemplary curves: 1. At the lowest end of Vm levels, the spiking tends to be close to zero and then around a certain voltage (threshold) it becomes positive. The rising phase of the curve around threshold voltage is nonlinear, as opposed to a strictly linear-threshold curve where the spiking should be zero below threshold and from threshold upward should vary linearly with Vm. 2. At the high end of the Vm values, spiking responses clearly saturate, heralding in the second nonlinear element in the V-F relationship. 3. The V-F relationships in the naïve and the experienced cells are very different in what range of Vm values the cells cover – the cells from

experienced animals go up to much higher voltages than the cells from naïve animals – and this leads to the experienced cells expressing much higher spiking rates than the naïve cells. 4. More interestingly, there is a distinct difference in slopes of the linear part of the fit curves between the two groups – the V-F curves are much steeper in the experienced animals than in naïve animals. 5. Finally, the Vm value at which the V-F curve touches zero spiking rate on the y axis (Vm intercept, a fit-based measure of spike threshold) is lower in the experienced cells.

We rigorously quantified the last two parameters for each cell as these could provide a biophysical link to why the V-F relationships in the two groups of cells look different. Slopes of the hyperbolic tangent fit from each cell were calculated by taking the peak derivative of the fitted curve. The average slope in the experienced group was significantly higher than the naïve group (**Figure 3C**; naïve: 3.692 +/- 0.636, n = 8 cells; experienced: 5.026 +/- 0.31, n = 15 cells; p = 0.03, WRS test). This signifies a clear enhancement of gain in the visually experienced animals, which would map the same membrane potential on to a higher spiking response. The Vm-intercept measure was significantly lower in the experienced group (**Figure 3D**; naïve: 5.26 +/- 0.89, n = 8 cells; experienced: 2.06 +/- 1.19, n = 15 cells; p = 0.03, WRS test). This signifies that the cells in the experienced animals start to fire spikes at a lower voltage on average, signifying that the biophysical threshold voltage may have been lowered, thereby enhancing spiking.

In order to get a complete picture of the developmental change in V-F relationship, we pooled the individual V-F curves from each cell within a category (naïve or experienced), binned them at 1mV intervals, and fitted the hyperbolic tangent function to these pooled data points. As a result, we obtained a single population average V-F curve for the naïve and the experienced groups each (**Figure 3E;** for complex cells, see **Supplementary Figure S7**). The population V-F

plots were fitted by the following hyperbolic tangent functions: naïve: FR = 20.8 + 21.4 * tanh((Vm – 19.1)/8.9)); experienced: FR = 21 + 20.3 * tanh((Vm – 13.9)/4.5)). These plots capture the essence of the result – the slope of the V-F relationship in the experienced group is much higher than in the naïve group, signifying a strong input-output gain enhancement with development.

To test the validity of our conjecture that enhanced V-F gain led to increased firing in the experienced cells, we projected the average Vm responses to preferred and null direction stimuli recorded in each cell on to the V-F plot fits from the same cells and predicted average firing responses. Comparison of the predicted and measured spiking responses revealed a strong significant correlation between the two, in both the naïve and experienced groups (**Figure 3F**; top: naïve, preferred direction: $R^2 = 0.93$, $p < 0.001$, null direction: $R^2 = 0.84$, $p = 0.001$; bottom: experienced, preferred direction: $R^2 = 0.78$, $p < 0.001$, null direction: $R^2 = 0.77$, $p < 0.001$). These strong correlations validate that our fitting of the V-F plots captured closely the essence of the cells' V-F relationships.

We earlier noted that, in the experienced animals, a modest increase in Vm responses to the preferred direction of motion led to a much stronger response at the spiking level (**Figure 1F**), leading to a robust developmental increase in spike DSI. Detection of a strong enhancement of input-output gain raised the possibility that this enhancement amplified the modest gains in Vm responses at the spiking level. To test this idea, we took the average total (i.e., F0+F1) Vm responses to preferred and null directions for each cell, and projected them on to both the naïve and the experienced population-average V-F fitted plots (**Figure 3E**), thereby generating spiking rate estimates for 4 conditions: naïve Vm projected on to naïve V-F, experienced Vm projected on to naive V-F, naive Vm projected on to experienced V-F and experienced Vm projected on to

experienced V-F. Among these, the naïve-on- experienced and experienced -on-naïve conditions allowed us to estimate what levels of spiking would be obtained if only input-output gain or Vm response gain had taken place, respectively. From these spiking estimates we calculated predicted spike DSI for each category. A comparison of these 4 categories of predicted spike DSI with the actually measured spike DSI in naïve and experienced animals (**Figure 3G**) revealed that only when experienced Vm was projected on to the experienced V-F plot, we obtained spike DSI predictions that were indistinguishable from the actually measured spike DSI in the experienced animals (one-way ANOVA, $F = 3.64$, $p = 0.006$; Fisher pot-hoc test p-value > 0.05 only for the experienced -on- experienced vs measured- experienced conditions). The predicted spike DSI for naïve-on- experienced and experienced -on-naïve conditions were both significantly lower than the measured experienced spike DSI (Fisher pot-hoc test p-value < 0.05). Therefore, an increase in Vm responses to the preferred direction of motion, presumably effected by the spatio-temporal input reorganizations (**Figure 2**), and an enhancement of input-output gain (**Figure 3**) were both required to account for the full extent of spike DSI increase during visual development.

Mechanisms of input-output gain enhancement: lowered spike threshold

What mechanisms underlie the sharp enhancement in input-output gain in the visually experienced animals? One idea is that the biophysical spike threshold of the neurons could be lowered during development (**Figure 4A**, left). The membrane potential undergoes spontaneous and stimulus-driven fluctuations, some of which takes it past the threshold voltage resulting in firing of action potentials. If the threshold voltage were lowered, the same Vm trace will now undergo more threshold-crossings and therefore lead to more spiking on average. Indeed, from analysis of V-F curves we learned that the average voltage at which the average spiking rate of

the neurons started to rise above zero – the Vm intercept – was lower in cells from the experienced animals (**Figure 3D**), suggesting that the threshold voltage on average might be lower in these animals. However, a more rigorous assessment of the threshold voltage for every single spike could be obtained by analyzing the shape of individual spikes. We employed a widely-used algorithm for such shape-based assessment of spike threshold[28-30]. **Figure 4B** shows the Vm trace of a neuron recorded during presentation of visual stimulus. The thresholds calculated for every single spike (see Supplementary methods) is superimposed on the corresponding spikes as red stars. For each simple cell included in the V-F analysis, we collected all spikes during presentation of the preferred-orientation stimulus, measured their threshold voltages, and averaged them to obtain a grand average spike threshold per cell. Comparing these cell-average values across the naïve and the experienced groups, we found a 20% reduction in spike threshold in the experienced animals (**Figure 4C**; naïve: 20.14 +/- 1.32 mV, n = 8; experienced: 16.05 +/- 0.9 mV, n = 15; p = 0.03, WRS test). These results, taken together with the fit-based assessment of threshold voltage (**Figure 3D**), strongly suggest that biophysical changes during visual development lower spike thresholds in simple cells, thereby allowing them to fire more spikes at a given Vm level.

The slope of the membrane potential (dV_m/dt) leading up to a spike is a reliable predictor of voltage-gated sodium current during spike upstroke, and therefore might control spike threshold[29,30]. If a high fraction of the voltage-gated sodium channels exists in the inactivated state, the sodium current decreases, thereby lowering the slope of rise of Vm (dV_m/dt). As a result, the maximum dV_m/dt reached before the onset of a spike is reduced, and the spike threshold is increased, as has been demonstrated in the cat V1[29,30]. To test if the lowered spike threshold observed in the visually experienced animals could have been caused by increased

maximum dV_m/dt before spike onset, we calculated the maximum slope of membrane potential in a 10-msec window before each action potential initiation, and computed an average maximum dV_m/dt value for each cell. When these values were compared across naïve and experienced animals, a 29% increase in maximum dV_m/dt was detected in the experienced group (**Figure 4D**; naïve: 200.7 +/- 15.8 volts/sec, n = 8, experienced: 257.8 +/- 13.4 volts/sec, n = 15; p = 0.01, WRS test). Therefore, in visually experienced animals, a steeper rise in Vm before an action potential led to lowering of spike threshold, thereby contributing to increased levels of firing for a given level of Vm.

Interestingly, we detected a similar developmental change in spike threshold and max dVm/dt in complex cells (see **Supplementary Figure S8**).

Mechanisms of gain enhancement: increased Vm oscillations

Like reduced spike threshold, increased variability or oscillations in the membrane potential could also lead to more threshold crossings (**Figure 4A**, right) and therefore higher spiking rates[29,31-34]. Membrane potential fluctuations, either during stimulus presentation or during inter-trial intervals, usually contain energy at various frequency bands. Amongst these, the high frequency (30-100Hz) gamma oscillations are particularly attractive candidate because i) highly synchronized synaptic inputs during visual stimulation could result in high frequency oscillations in Vm, and ii) more frequent or variable rises in Vm are more likely to cause spiking[32-34]. Therefore, to test if the neurons in the experienced animals contained stronger gamma oscillations in Vm, we carried out Fourier analysis of the spike-filtered Vm traces during presentation of stimulus at the preferred orientation (see **Supplementary Methods**). **Figure 5A** shows the power in Vm oscillations in the 1-100Hz range for all simple cells. It is evident from the figure that the Vm contained higher power in the gamma frequencies during stimulus

presentation in the experienced animals. To quantify the gamma power, we integrated the Vm power over the entire gamma frequency range (30-100Hz) for each individual trial, and averaged the integrated gamma power for all trials within each cell to obtain an average integrated gamma power per cell. Compared to the naïve group, integrated gamma power per cell was significantly higher in the experienced group (**Figure 5B**; $p = 0.016$, WRS test). Furthermore, consistent with the idea that higher gamma oscillations in Vm during visual stimulation could lead to higher levels of spiking, we found a strong linear correlation between Vm gamma power and spike rates, both at the levels of single trials and single cells (**Figure 5C**). This correlation was significant in both the naïve and experienced groups (per trial: naïve: $R^2 = 0.74$, $p < 0.001$; experienced: $R^2 = 0.41$, $p < 0.001$; per cell: naïve: $R^2 = 0.77$, $p = 0.002$; experienced: $R^2 = 0.5$, $p = 0.002$). However, Vm gamma power in cells from experienced animals often reached very high values during many trials, thereby giving a bigger boost to overall spiking in the experienced group. A small but significant increase in gamma power was also observed in complex cells (**Supplementary Figure S9**). Therefore, in addition to reduced spike thresholds, increased high-frequency oscillations in Vm could also have contributed to increased levels of spiking in the visually experienced animals.

Discussion

We studied the evolution of input-output transformation during visual development of V1 simple cells by mapping out input patterns and neuronal input-output functions through in vivo intracellular recordings. Shape analysis of linear spatio-temporal receptive fields (STRFs) of simple cells in visually naïve and experienced ferrets showed that the elliptical STRF subunits in experienced animals exhibit more eccentric profiles and contain inputs with shorter latencies not seen in naïve animals. This synaptic reorganization led to improved summation of subthreshold inputs, resulting in a small but significant increase in direction selectivity at the level of Vm. Analysis of the Vm-to-spiking transfer relationship in the same neurons revealed that the slope of the Vm-spike relationship increased in the experienced animals, signifying that for the same average Vm levels in naïve and experienced animals, there was more spiking output in the experienced state. The full extent of DSI increases at the spiking level could only be explained by considering both the small enhancement in Vm direction selectivity and the enhancement of input-output gain. We explored two possible mechanisms for enhancement of spiking in experienced neurons, namely, lowering of spike threshold and increased Vm variability via high-frequency Vm oscillations. Spike thresholds were found to be on 4 mV lower on average in the experienced animals, and there was a significant increase in power in the gamma-band of Vm oscillations, implying that both mechanisms contribute to increased spiking in experienced neurons. Taken together, these results outline a scenario for direction selectivity development that includes two critical components: first, rearrangement in spatio-temporal patterns of inputs to simple cells produces slightly more directionally-selective Vm responses, and second, these modestly enhanced Vm responses then map on to a steeper Vm-to-spike input-output curve, thereby producing an even more directionally-selective spiking response.

In the linear receptive fields of simple cells, optimal directional computation is achieved by making the spatial and temporal properties inseparable, meaning that strong synaptic inputs exist only at certain combinations of spatial position and temporal latencies and that they vary systematically across the space-time axes. STRF mapping in simple cells with low direction selectivity of visually naïve ferrets revealed weaker inseparability, leading to broader STRF subunits that contained inputs with a wider range of spatial and temporal combinations. However, the naïve STRFs were not completely devoid of structure, and displayed inputs well-organized into a coherent structure, including even a weak slant in space-time which may explain the small direction selectivity observed at the Vm level in these cells. Over visual development, the set of strong inputs winnows down to a narrower range of space-time combinations, presumably through synaptic pruning, consequently giving rise to more eccentric STRF subunits. This more eccentric space-time organization of inputs allows optimal input summation for the preferred direction of motion only and thus leads to enhanced Vm DSI.

The non-linear relationship between Vm and spiking in V1 simple cells is well-established. This results in higher spike DSI compared to Vm DSI in individual cells, as we observed in our data. However, during development, the gain of this non-linearity could increase, further enhancing DSI at the spiking level. Our examination of the Vm-to-spike transfer functions across visually naïve and experienced stages of development corroborated this idea: for increasing average Vm levels, spiking increased with a steeper slope in the experienced animals. Gain enhancement implied that the relatively larger Vm levels attained during the preferred direction of motion mapped on to a much higher level of spiking in the experienced animals, thereby amplifying spike DSI. By cross-projecting naïve and experienced Vm responses on to the naïve and experienced V-F plots, we found that the developmental enhancements of subthreshold

responses alone are not sufficient to account for the full range of increase in spike DSI; instead, both subthreshold increases and enhancement of input-output gain must be considered. These results imply that circuit-wide synaptic reorganizations must work in sync with dynamics of cell-intrinsic properties during development to give rise to mature functional properties such as direction selectivity.

Although the composition of voltage-gated ionic channels in the cell membrane, specifically in the axon initial segment (AIS), and the location of the AIS with respect to the soma, dictate a neuron's biophysical threshold potential for firing spikes[35-37], the threshold voltage can dynamically vary depending on the manner in which synaptic inputs modulate the neuron's membrane potential[29,30]. For example, convergence of synchronized excitatory inputs, as induced by a sensory stimulus, could produce a sharp rise, and therefore a steeper slope, in the membrane potential, leading to lowering of spike threshold. This contrasts with baseline conditions, when temporally disorganized spontaneous inputs can elevate the Vm to similar average levels but with a shallower slope, and therefore not achieve a lowered spike threshold. This possibility of dynamic regulation of spike threshold makes it an attractive mechanism for controlling a neuron's excitability. Our observation that the spike threshold in the experienced ferrets were ~20% lower relative to rest than in the naïve ferrets makes a strong case for threshold dynamics playing a key role in enhancing the input-output gain in the experienced state. Furthermore, the increased maximum slope of the Vm preceding a spike in the experienced state also suggests enhancement of sodium current during the spike upstroke as a possible reason for lowering of threshold voltage[29,30]. Sensory activity has been shown to drive changes in the location of and the composition of voltage-gated sodium channel subunits in the AIS[38,39], and such channel dynamics can cause sodium current to increase in the experienced state. Future studies will

address if and how visual activity might modulate such channel dynamics and consequently control intrinsic excitability of simple cells.

Altered Vm oscillations in the gamma band has been implicated in state-dependent modifications of firing levels in cortical neurons[29,31,40]. We found a notable increase in Vm gamma power in the visually experienced animals. Because gamma oscillations are shaped by state-dependent changes in network activity, and brain states could vary between stimulus trials, trial-to-trial variation in firing rates could be driven by trial-to-trial variation in Vm gamma power. Consistent with this idea, we found evidence for a strong linear correlation between Vm gamma power and firing rate for each stimulus trial, in both naïve and experienced animals. This relationship held true even at the single cell level. Combined with the observation that, on average, Vm gamma power values were higher in the experienced animals as compared to the naïve animals, these data suggest that increased high-frequency Vm oscillations could constitute one plausible explanation for enhanced spiking activity in the experienced animals. Strengthening of the cortical inhibitory network and the neuromodulatory circuits during development could underlie the increased gamma oscillations in the network, and will be the focus of future studies exploring the mechanistic underpinnings of input-output gain enhancement.

Methods Summary

Ferrets were anesthetized with ketamine and isoflurane (2% for surgery, 0.08-2% during imaging). Intracellular recordings from V1 neurons were performed using sharp microelectrodes (80-120 megaohms) and an AxoClamp 2B amplifier (Molecular Devices, CA) in the bridge mode. Linear spatiotemporal receptive fields (STRFs) were computed by reverse-correlating membrane potential (Vm) responses to a sparse white noise stimulus. Input-output transfer curves for neurons were computed by plotting average spike rates against corresponding average levels of Vm values. Threshold voltages for individual action potentials were measured by finding the Vm value preceding a spike at which the slope of the Vm (dVm/dt) reached 3% of its maximum value. To measure high-frequency Vm oscillations, spike-filtered Vm traces during visual stimulation were analysed with fast Fourier transformation and the power in the gamma-band were calculated by integrating the squares of the FFT amplitudes in the 30-100 Hz frequency range. Stimulation and analysis were performed using custom software for Matlab (MathWorks). See **Supplementary Information** for details.

Figures and legends

Figure 1

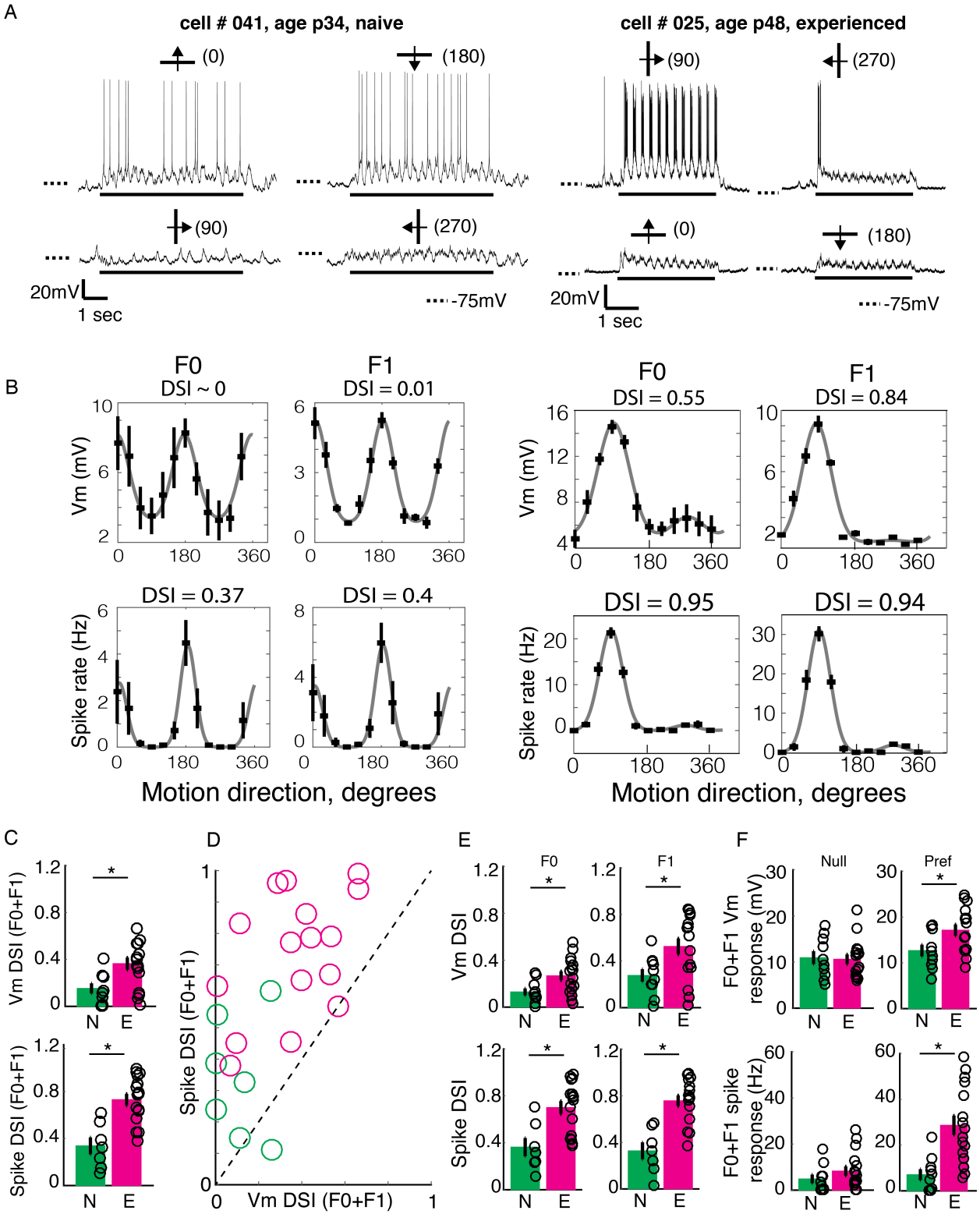

Figure 1. Developmental increase in direction selectivity of membrane potential (Vm) and spiking responses in V1 simple cells. A. Vm responses of a simple cell from a visually naïve and an experienced ferret each. For each cell, single-trial responses to presentation of sinusoidal gratings moving in both directions orthogonal to the preferred orientation (top) and the non-preferred orientation (bottom) are shown. The stimulus orientations and motion directions are indicated above each trace with a solid bar and arrow, respectively, and the angles representing the specific directions of motion are given in parentheses. Solid bar below each trace indicate the duration of the stimulus display and dotted lines indicate the Vm level of -75 mV. For both cells, the gratings drifted at a temporal frequency of 4 Hz and the Vm oscillated at the same frequency with a strong response to each grating cycle. **B.** Direction tuning curves of the cells in A, plotted separately for Vm (top) and spiking (bottom) responses, and for the F0 or DC (left) and the F1 or fundamental (right) components of the responses. Direction selectivity index (DSI) calculated from each tuning curve is given above each curve. Both F0 and F1 DSI values are higher in the cell from the experienced animal. **C.** Mean total Vm and spike DSI values, calculated from F0+F1 responses, compared between naïve (N, green) and experienced (E, purple) animal groups. **D.** Vm and spike total DSI (F0+F1) values for each simple cell plotted against each other. Dashed line denotes the line of unity. **E.** Same as C, but the DSI values are calculated separately for the F0 and the F1 components of response. **F.** Mean total (F0+F1) Vm and spiking responses to the null and preferred direction of motion compared between naïve and experienced groups. For all panels: error bars denote SEM; circles denote values for individual cells; asterisks denote significant differences at $p < 0.05$ level, Wilcoxon rank sum test.

Figure 2

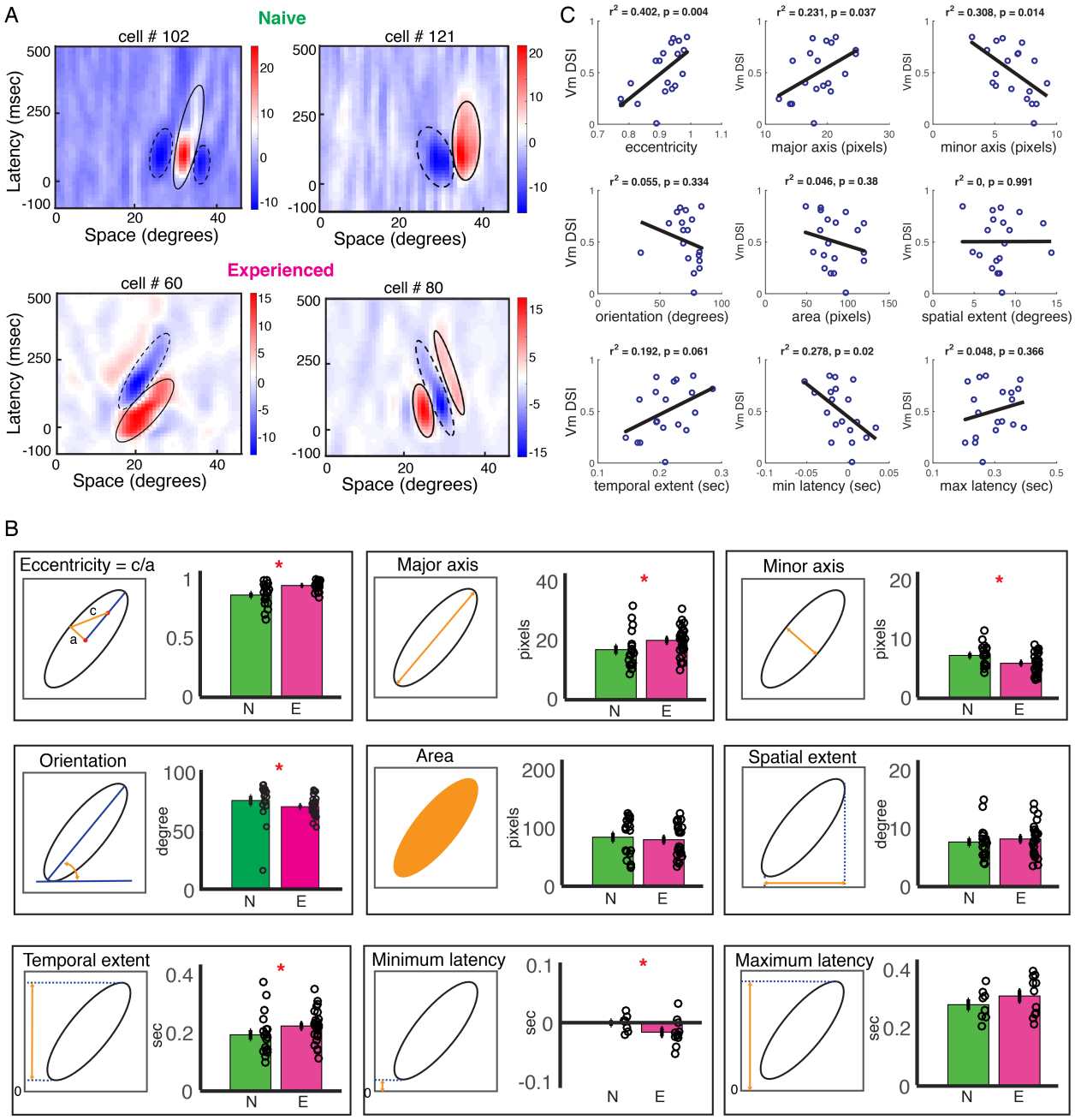

Figure 2. Developmental reorganization of linear spatiotemporal receptive fields (STRFs) in V1 simple cells. A. Vm STRFs of two simple cells each from naïve (top, cell # 102, 121) and experienced (bottom, cell # 60, 80) animals. X-axis represents spatial location, y-axis represents latency from onset of visual stimulus, and the cross-correlation coefficient between the stimulus contrast and Vm values are represented by the color. Black lines outline the ellipses fitted to the ON (continuous) and OFF (dashed) subunits. **B.** Quantification of the 9 parameters defining the characteristics of the STRF subunits, organized in 3 rows and 3 columns. In each panel, the

parameter being quantified is described by a schematic on the left, and on the right is a bar plot showing the mean +/- SEM of the parameter values in the naïve (N, green, 19 subunits from 8 cells) and experienced (E, purple, 26 subunits from 12 cells) animals. Black circles denote individual subunit values. Red stars denote statistical significance at $p < 0.05$ level via WRS test. **C.** Relationship between cell-average STRF structure parameters and Vm DSI for all simple cells. The R^2 and p values for each linear correlation are shown above each plot.

Figure 3

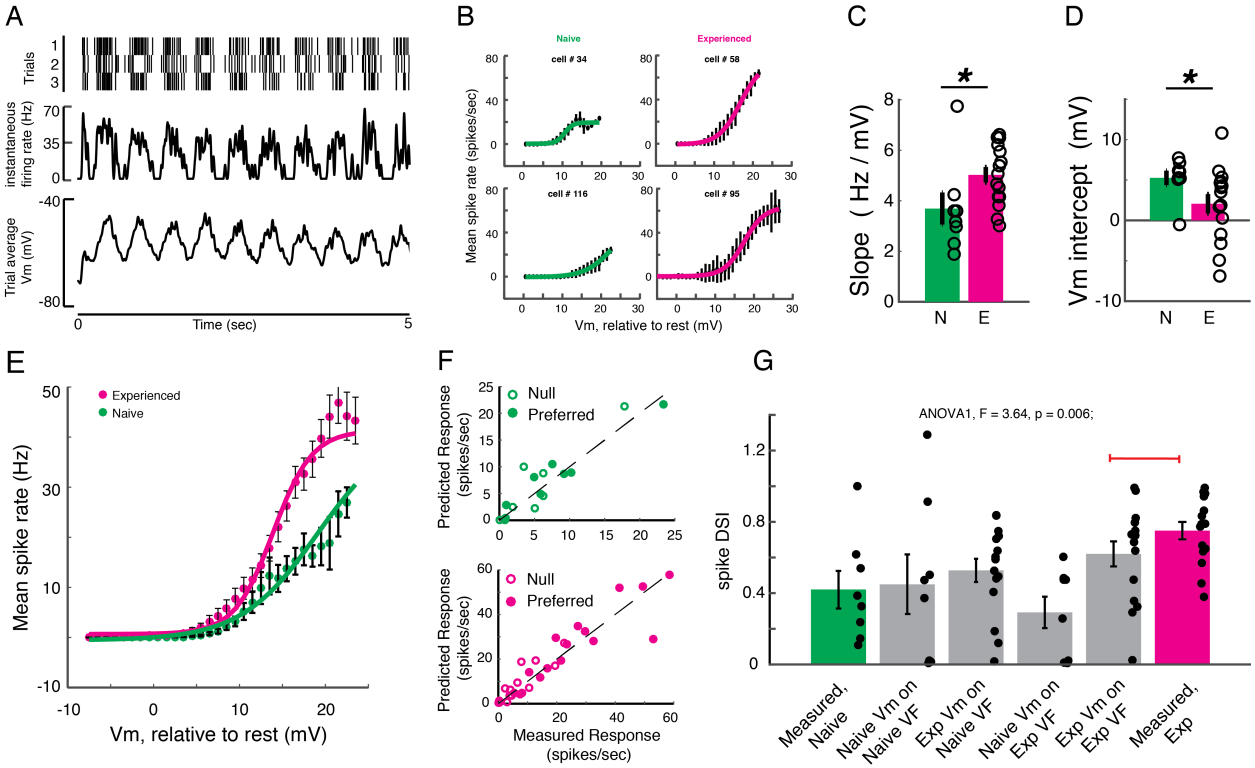

Figure 3. Developmental enhancement of input-output gain in V1 simple cells. A. Methodology of uncovering the input-output (V-F) relationship. *Top*: raster plots of spikes fired during 3 trials of stimulus presentation, *middle*: instantaneous firing rate obtained by binning the rasters, *bottom*: trial-averaged membrane potential trace during the same period. Vm values and corresponding firing rates between the bottom and the middle panels were used to generate the V-F plots. **B.** V-F plots of 2 cells each from naïve and experienced animals. **C.** Comparison of the slope of the linear portion of the hyperbolic tangent fits to the V-F plots. Bars represent mean +/- SEM slope values in naïve (N, green) and experienced (E, purple) groups. Each circle shows individual cell values. **D.** Comparison of the Vm values where the V-F curve intercepts the x axis (i.e., y = 0). Bars represent mean +/- SEM intercept values in naïve (N, green) and experienced (E, purple) groups. Each circle shows individual cell values. **E.** Population average V-F plots in naïve and experienced animals. **F.** For every simple cell, the predicted spiking responses to preferred (solid circles) and null (open circles) direction motions obtained from the V-F plots are plotted against the experimentally measured spiking responses, for naïve (top) and experienced (bottom) animals. Unity line shown in dashes. **G.** Experimentally measured spike DSIs and spike DSIs predicted from a combinatorial projection of average naïve and experienced Vm responses on to average naïve and experienced V-F plots. Each circle represents the corresponding value for a single cell. Following a significant one-way ANOVA, the experimentally measured spike DSI in the experienced group (purple bar) was pair-wise compared to all the other 5 categories using Fisher's post-hoc test. The red line denotes the only comparison where p value of the Fisher's test was > 0.05.

Figure 4

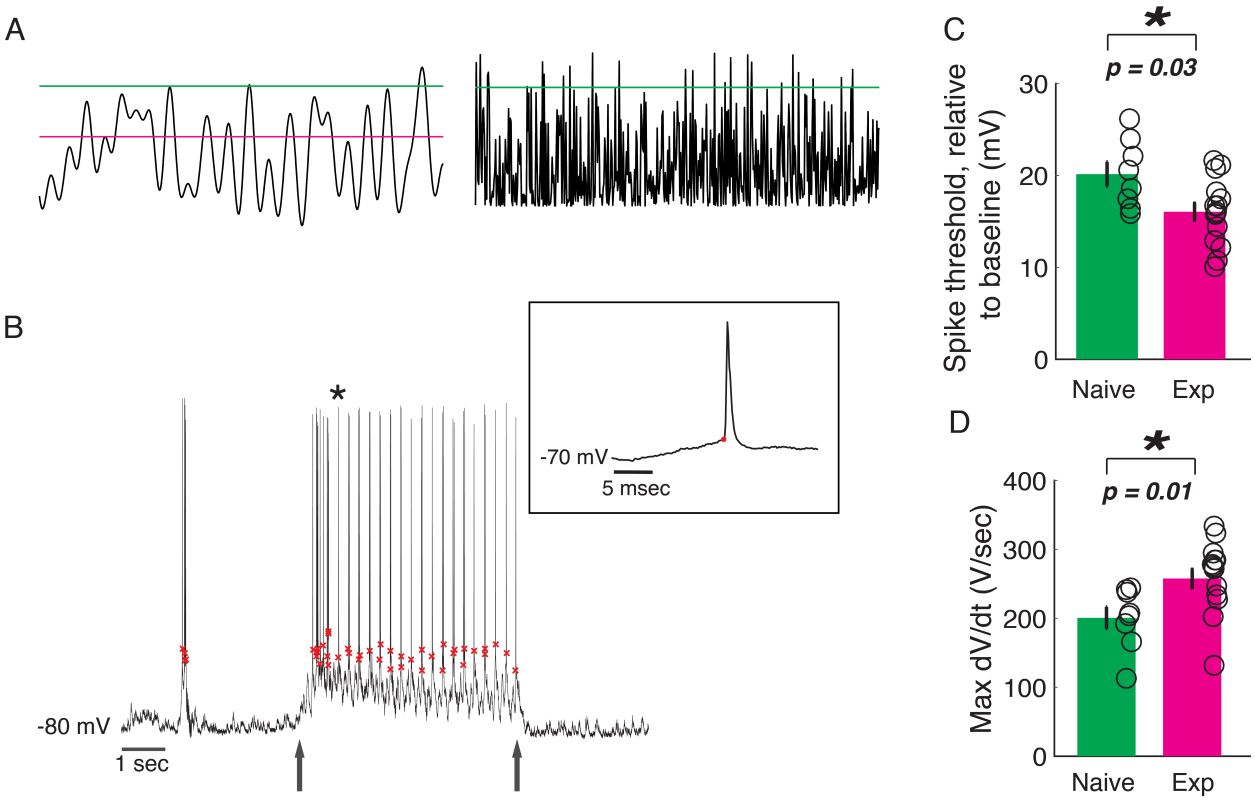

Figure 4. Developmental lowering of spike threshold in V1 simple cells. A. For the same average level of Vm, spike rate could be increased either by lowering the spike threshold (left) or by increasing the high-frequency oscillations in Vm (right). In the first scenario, the same Vm trace (black) would cross threshold voltage more often if the spike threshold in the experienced cells (purple line) were lower compared to that in the naïve cells (green line). In the second scenario, if the Vm (black) undergoes more high-frequency oscillations in the experienced animals while keeping the threshold (green line) same, increased threshold crossings can also be achieved. **B.** An example raw Vm trace during stimulus presentation (gray arrows). The calculated spike threshold voltages for every spike in the trace shown as red asterisks, demonstrating the variability in spike thresholds. The inset shows a zoomed in view of one spike marked by the black asterisk and its threshold voltage precisely at the point where Vm rises sharply. **C.** Comparison of the threshold voltages. Bars represent mean +/- SEM thresholds in naïve (green) and experienced (purple) groups. Each circle shows individual cell values. **D.** Comparison of the maximum slope of Vm preceding spikes. Bars represent mean +/- SEM max dV/dt values in naïve (green) and experienced (purple) groups. Each circle shows individual cell values.

Figure 5

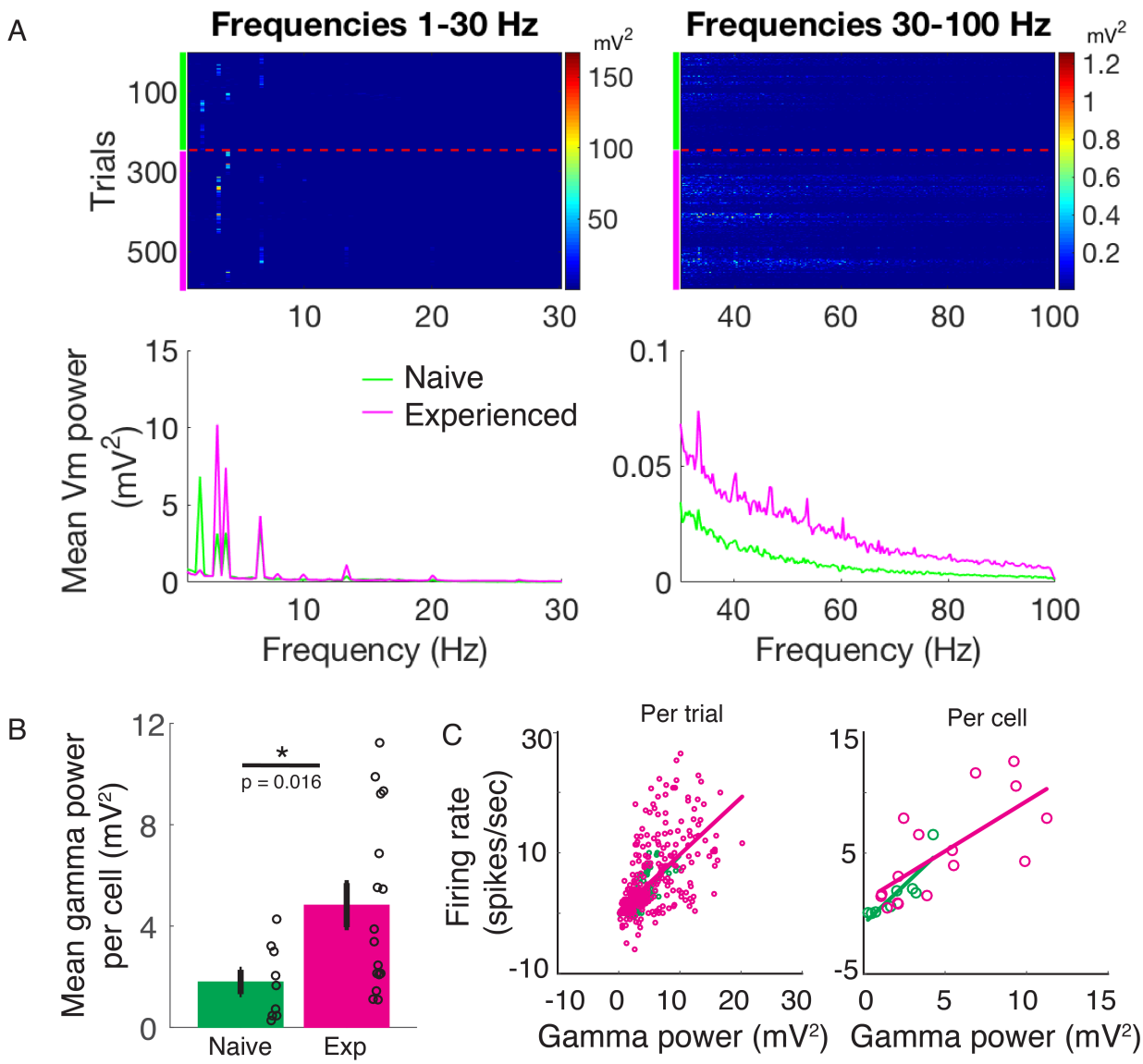

Figure 5. Developmental increase of high-frequency Vm oscillations in V1 simple cells. A. Top: the power in Vm oscillations are plotted for the entire frequency range of 1-100Hz for all simple cells, each row representing single trials and the trials from the naïve animals arranged on the top (green bar on left side). While at the lower frequencies (1-30Hz, containing theta and beta bands) the power is dominated by the oscillations at the stimulus temporal frequency and its harmonics, in gamma band (30-100Hz) the power of Vm fluctuations can be seen un-corrupted by stimulus-locked oscillations. Bottom: average power at each oscillation frequency, obtained by averaging across trials in each group. **B.** The average integrated gamma power per cell in naïve and experienced animals. **C.** Linear correlation between Vm gamma powers and spike rates for every trial (left) and for every cell (right) in the naïve and experienced groups.

References

1 Hubel, D. H. & Wiesel, T. N. Receptive fields of single neurones in the cat's striate cortex. *J Physiol* **148**, 574-591 (1959).

2 Hubel, D. H. & Wiesel, T. N. Receptive Fields And Functional Architecture In Two Nonstriate Visual Areas (18 And 19) Of The Cat. *J Neurophysiol* **28**, 229-289 (1965).

3 Shmuel, A. & Grinvald, A. Functional organization for direction of motion and its relationship to orientation maps in cat area 18. *J Neurosci* **16**, 6945-6964 (1996).

4 Chapman, B. & Stryker, M. P. Development of orientation selectivity in ferret visual cortex and effects of deprivation. *J Neurosci* **13**, 5251-5262 (1993).

5 Li, Y., Fitzpatrick, D. & White, L. E. The development of direction selectivity in ferret visual cortex requires early visual experience. *Nat Neurosci* **9**, 676-681 (2006).

6 White, L. E., Coppola, D. M. & Fitzpatrick, D. The contribution of sensory experience to the maturation of orientation selectivity in ferret visual cortex. *Nature* **411**, 1049-1052, doi:10.1038/35082568

35082568 [pii] (2001).

7 Humphrey, A. L. & Saul, A. B. Strobe rearing reduces direction selectivity in area 17 by altering spatiotemporal receptive-field structure. *J Neurophysiol* **80**, 2991-3004 (1998).

8 Li, Y., Van Hooser, S. D., Mazurek, M., White, L. E. & Fitzpatrick, D. Experience with moving visual stimuli drives the early development of cortical direction selectivity. *Nature* **456**, 952-956, doi:10.1038/nature07417 (2008).

9 Smith, G. B. *et al.* The development of cortical circuits for motion discrimination. *Nat Neurosci* **18**, 252-261, doi:10.1038/nn.3921 (2015).

10 McLean, J., Raab, S. & Palmer, L. A. Contribution of linear mechanisms to the specification of local motion by simple cells in areas 17 and 18 of the cat. *Visual Neurosci.* **11**, 271-294 (1994).

11 Reid, R. C., Soodak, R. E. & Shapley, R. M. Linear mechanisms of directional selectivity in simple cells of cat striate cortex. *Proc Natl Acad Sci U S A* **84**, 8740-8744 (1987).

12 Reid, R. C., Soodak, R. E. & Shapley, R. M. Directional selectivity and spatiotemporal structure of receptive fields of simple cells in cat striate cortex. *J Neurophysiol* **66**, 505-529 (1991).

13 Priebe, N. J. & Ferster, D. Direction selectivity of excitation and inhibition in simple cells of the cat primary visual cortex. *Neuron* **45**, 133-145, doi:S0896627304008402 [pii] 10.1016/j.neuron.2004.12.024 (2005).

14 Priebe, N. J., Mechler, F., Carandini, M. & Ferster, D. The contribution of spike threshold to the dichotomy of cortical simple and complex cells. *Nat Neurosci* **7**, 1113-1122 (2004).

15 Jagadeesh, B., Wheat, H. S. & Ferster, D. Linearity of summation of synaptic potentials underlying direction selectivity in simple cells of the cat visual cortex. *Science* **262**, 1901-1904 (1993).

16 DeAngelis, G. C., Ohzawa, I. & Freeman, R. D. Spatiotemporal organization of simple-cell receptive fields in the cat's striate cortex. II. Linearity of temporal and spatial summation. *J. Neurophysiol.* **69**, 1118-1135 (1993).

17 DeAngelis, G. C., Ohzawa, I. & Freeman, R. D. Spatiotemporal organization of simple-cell receptive fields in the cat's striate cortex. I. General characteristics and postnatal development. *J. Neurophysiol.* **69**, 1091-1117 (1993).

18 Carandini, M. & Ferster, D. Membrane potential and firing rate in cat primary visual cortex. *J Neurosci* **20**, 470-484 (2000).
19 Mechler, F. & Ringach, D. L. On the classification of simple and complex cells. *Vision Res* **42**, 1017-1033 (2002).
20 van Kleef, J. P., Stange, G. & Ibbotson, M. R. Applicability of white-noise techniques to analyzing motion responses. *J Neurophysiol* **103**, 2642-2651, doi:10.1152/jn.00591.2009 (2010).
21 Ringach, D. L., Sapiro, G. & Shapley, R. A subspace reverse-correlation technique for the study of visual neurons. *Vision Res* **37**, 2455-2464, doi:S0042-6989(96)00247-7 [pii] (1997).
22 Reid, R. C., Victor, J. D. & Shapley, R. M. The use of m-sequences in the analysis of visual neurons: linear receptive field properties. *Vis Neurosci* **14**, 1015-1027 (1997).
23 Livingstone, M. S. Mechanisms of direction selectivity in macaque V1. *Neuron* **20**, 509-526, doi:10.1016/s0896-6273(00)80991-5 (1998).
24 Reichardt, W. & Poggio, T. Visual control of orientation behaviour in the fly. *Quart. Rev. Biophys.* **9**, 311-375 (1976).
25 Reichardt, W. Evaluation of optical motion information by movement detectors. *J. Comp. Physiol. A* **161**, 533-547 (1987).
26 Leong, J. C., Esch, J. J., Poole, B., Ganguli, S. & Clandinin, T. R. Direction Selectivity in Drosophila Emerges from Preferred-Direction Enhancement and Null-Direction Suppression. *J Neurosci* **36**, 8078-8092, doi:10.1523/JNEUROSCI.1272-16.2016 (2016).
27 Tavazoie, S. F. & Reid, R. C. Diverse receptive fields in the lateral geniculate nucleus during thalamocortical development. *Nat Neurosci* **3**, 608-616 (2000).
28 Azouz, R. & Gray, C. M. Cellular mechanisms contributing to response variability of cortical neurons. *J. Neurosci.* **19**, 2209-2223 (1999).
29 Azouz, R. & Gray, C. M. Dynamic spike threshold reveals a mechanism for synaptic coincidence detection in cortical neurons in vivo. *Proc. Natl. Acad. Sci. USA* **97**, 8110-8115 (2000).
30 Azouz, R. & Gray, C. M. Adaptive coincidence detection and dynamic gain control in visual cortical neurons in vivo. *Neuron* **37**, 513-523, doi:10.1016/s0896-6273(02)01186-8 (2003).
31 Polack, P. O., Friedman, J. & Golshani, P. Cellular mechanisms of brain state-dependent gain modulation in visual cortex. *Nat Neurosci* **16**, 1331-1339, doi:10.1038/nn.3464 (2013).
32 Brunel, N., Chance, F. S., Fourcaud, N. & Abbott, L. F. Effects of synaptic noise and filtering on the frequency response of spiking neurons. *Phys Rev Lett* **86**, 2186-2189, doi:10.1103/PhysRevLett.86.2186 (2001).
33 Chance, F. S., Abbott, L. F. & Reyes, A. D. Gain modulation from background synaptic input. *Neuron* **35**, 773-782, doi:10.1016/s0896-6273(02)00820-6 (2002).
34 Finn, I. M., Priebe, N. J. & Ferster, D. The emergence of contrast-invariant orientation tuning in simple cells of cat visual cortex. *Neuron* **54**, 137-152, doi:S0896-6273(07)00169-9 [pii] 10.1016/j.neuron.2007.02.029 (2007).
35 Hu, W. *et al.* Distinct contributions of Na(v)1.6 and Na(v)1.2 in action potential initiation and backpropagation. *Nat Neurosci* **12**, 996-1002 (2009).
36 Colbert, C. M. & Pan, E. Ion channel properties underlying axonal action potential initiation in pyramidal neurons. *Nat Neurosci* **5**, 533-538, doi:10.1038/nn857 (2002).

37 Kole, M. H. *et al.* Action potential generation requires a high sodium channel density in the axon initial segment. *Nat Neurosci* **11**, 178-186, doi:10.1038/nn2040 (2008).
38 Grubb, M. S. & Burrone, J. Activity-dependent relocation of the axon initial segment fine-tunes neuronal excitability. *Nature* **465**, 1070-1074, doi:10.1038/nature09160 (2010).
39 Kuba, H., Oichi, Y. & Ohmori, H. Presynaptic activity regulates Na(+) channel distribution at the axon initial segment. *Nature* **465**, 1075-1078, doi:10.1038/nature09087 (2010).
40 Bennett, C., Arroyo, S. & Hestrin, S. Subthreshold mechanisms underlying state-dependent modulation of visual responses. *Neuron* **80**, 350-357, doi:10.1016/j.neuron.2013.08.007 (2013).